Self-Assembly of Polypeptide/π-Conjugated Polymer/Polypeptide Triblock Copolymers in Rod−Rod−Rod and Coil−Rod−Coil Conformations

Laurent Rubatat,[†,#] Xiangxing Kong,[‡] Samson A. Jenekhe,[‡] Janne Ruokolainen,[§] Mohamad Hojeij,[||] and Raffaele Mezzenga[⊥,*,†]

Department of Physics and Fribourg Center for Nanomaterials, Fribourg University, Fribourg, Switzerland; Department of Chemical Engineering, University of Washington, Seattle, Washington 98195-1750; Helsinki University of Technology, Espoo, Finland; Laboratoire d'Electrochimie Physique et Analytique, Ecole Polytechnique Fédérale de Lausanne, Station 6, CH-1015 Lausanne, Switzerland; and Néstlé Research Center, Vers-Chez-Les-Blanc, 1000 Lausanne 26, Switzerland

Received October 12, 2007; Revised Manuscript Received December 5, 2007

ABSTRACT: Self-assembly in the bulk of a series of hybrid triblock copolymers formed by a poly(9,9-dihexylfluorene-2,7-diyl) (PHF) middle block and two poly(γ-benzyl-L-glutamate) (PBLG) end blocks has been studied. Since the α-helical secondary structure of the PBLG block may be either maintained or suppressed depending on the solvent casting history, the PBLG−PHF−PBLG copolymers exhibit two different conformations: a rod−rod−rod or coil−rod−coil configuration, respectively. In order to provide insight into the influence of conformation on self-aggregation of these systems, three copolymers with different block ratio were investigated in both conformations using small- and wide-angle scattering techniques and transmission electron microscopy. Time-resolved photoluminescence measurements were performed on the same samples to explore the effect of morphology on photophysical properties. The observed photoluminescence spectra and dominant excited lifetimes of the poly(9,9-dihexylfluorene-2,7-diyl) block were found to differ markedly in rod−rod−rod and coil−rod−coil configurations and were correlated to the morphology of the self-assembled triblock copolymers.

Introduction

During the past decade, a large number of papers have been devoted to the study of the rod−coil class of block copolymers, where the rod block provides the additional effect of liquid crystalline behavior in the self-assembly of block copolymers.[1−3] Although the phase diagram of the coil−coil copolymers is now well understood both experimentally and theoretically,[4−6] the rod−coil self-assembly is still under intensive theoretical and experimental investigation.[2,7−9] Recently, in view of more controlled morphologies and enhanced properties, more complicated molecular architectures such as rod−rod diblock copolymer[10,11] or rod−coil−rod[12] and coil−rod−coil[13,14] triblock copolymers have also become the object of several studies. The rigidity of the rod blocks can be achieved either by polypeptides exhibiting α-helical secondary structure or with π-conjugated polymers. Both classes of systems are of interest for advanced applications. Indeed, while polypeptides provide, to a certain extent, biocompatibility such as in 3D scaffolds for tissue engineering and biomineralization, π-conjugated polymers are appealing systems for their optoelectronic and photoconductive properties.[15] Recently, Kong and Jenekhe reported the synthesis of a novel hybrid π-conjugated-based ABA triblock copolymer.[16] These hybrid triblock copolymers containing a middle conjugated polymer block and two end polypeptide blocks are expected to improve the interaction between the electro- and photoactive blocks with biomolecules. Consequently, applications such as wires for delivering electrical stimuli to influence cell growth and cell morphology[17] or such as biosensors[18,19] can be considered.

In the present paper, we continue the work initiated by Kong and Jenekhe reporting on the bulk ordering of a homologue series of hybrid ABA triblock copolymers containing poly(9,9-dihexylfluorene-2,7-diyl) (PHF) and poly(γ-benzyl-L-glutamate) (PBLG). From a structural point of view these systems are remarkable since poly(γ-benzyl-L-glutamate) can exhibit both α-helical secondary structure, which confers rodlike behavior or coil configuration. The rod−coil transition can be triggered by (i) varying the temperature at a constant solvent composition or (ii) by varying the solvent composition at constant temperature.[20] The commonly used unwinding agents are dichloroacetic acid (DCA)[20,21] and trifluoroacetic acid (TFA).[16,22] Roots et al. have shown that in a solution of DCA/dichloroethane (80/20 w/w) the PBLG coil form is most stable below 20 °C and the helix form is dominant above 40 °C; the transition temperature is found to be 31 °C.[21] The morphology of block copolymers containing PBLG blocks, with different molecular architecture, has also been investigated in solution[23] and in bulk.[24,25] These studies discuss the structural modification occurring during the self-assembly of the block copolymer after the rod-to-coil transition of the PBLG block. Polyfluorenes, the middle block of the triblock copolymers studied in the present work, are intensively investigated in the literature due to their potential for blue organic light-emitting diodes (OLEDs).[26] Despite its poor spectral stability ranging from blue to blue-green emission,

* To whom correspondence should be addressed. University of Fribourg: e-mail raffaele.mezzenga@unifr.ch, Tel + 41 26 300 9066, Fax + 41 26 300 9747; Nestlé Research Center: e-mail raffaele.mezzenga@rdls.nestle.com, Tel + 41 21 785 8078, Fax + 41 21 785 8554.
† Fribourg University.
‡ University of Washington.
§ Helsinki University of Technology.
|| Ecole Polytechnique Fédérale de Lausanne.
⊥ Néstlé Research Center.
New address: Département de Physique, UMR IPREM 5254, Université de Pau, 64000 Pau Cedex, France.

10.1021/ma702278a CCC: $40.75
Published on Web 02/12/2008

Scheme 1. (a) Chemical Structure of the PBLG−PHF−PBLG Triblock Copolymer; (b) Schematic Representation of the Three Different Triblocks[a]

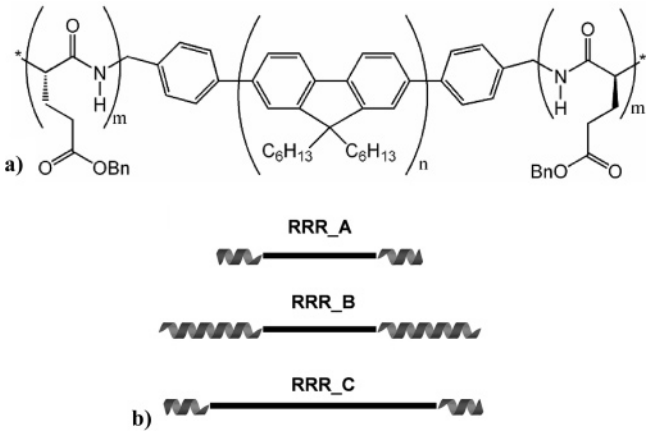

[a] The *Bn* notation corresponds to a benzyl group. The contour length proportions are respected for the rod−rod−rod configuration.

Table 1. Triblock Copolymer Description

samples	PBLG M_w	PHF M_w	PBLG contour length[a] (nm)	PHF contour length[b] (nm)
A	5000	5000	3.45	12.6
B	13000	5000	8.1	12.6
C	4000	9000	2.4	23.5

[a] PBLG α-helix contour length is calculated considering that one unit contributes to 1.5 Å.[37] [b]PHF contour length is calculated by using Chem3D.[16]

polyfluorenes are still good candidates for blue OLEDs thanks to their high photoluminescence quantum yields, in the solid state, and good charge transport properties.[26] In order to eliminate or attenuate the green emission, other components have been tentatively blended with polyfluorene, such as poly(vinyldiphenylquinoline).[27] Alternatively, also the tuning of the structure by using multiblock copolymers where the polyfluorene constitutes at least one block has been explored.[28−30]

In this paper, we report investigation of three PBLG−PHF−PBLG triblock copolymers with various block ratios in their two possible conformations: rod−rod−rod (RRR series) and coil−rod−coil (CRC series). The morphologies were observed in real space using transmission electron microscopy (TEM) and correlated with reciprocal space data using small- and wide-angle X-ray scattering (SAXS and WAXS). Steady-state and time-resolved photoluminescence spectra were measured on the samples and correlated with the morphology.

Experimental Section

Sample Preparation. The chemical structure of the triblock copolymers containing poly(9,9-dihexylfluorene-2,7-diyl) (PHF) and poly(γ-benzyl-L-glutamate) (PBLG), denoted BLG*m*-HF*n*-BLG*m*, is shown in Scheme 1a. The polymers were synthesized by ring-opening polymerization of the PBLG blocks on PHF macroinitiators. The PHF macroinitiators were prepared by Yamamoto coupling polymerization. More details on the synthesis are reported in ref 16. Three block copolymers with different degree of polymerization are prepared: *m*/*n* 23/15 (same as in ref 16), 54/15, and 16/28 (same as in ref 16); see Table 1. Chloroform is used to cast the samples in the rod−rod−rod conformation since it is a good solvent for both blocks and does not denature the α-helix of the polypeptide. The coil−rod−coil conformation is obtained by unwinding the PBLG helix using a mixture of chloroform and tretafluoroacetic acid (TFA), 75/25 by weight.[16,22] Physical characterization of the triblock copolymers was carried out on samples annealed at 160 °C for 72 h under a 5×10^{-11} bar vacuum.

Table 2. Results on the Coil−Rod−Coil Samples from the TEM Micrographs Analysis Using the Technique Described by Sary et al.[31]

samples	periods (nm)	black lamellae[a] (nm)	white lamellae[a] (nm)
CRC_A	35 ± 6	19 ± 3	16 ± 3
CRC_B	23 ± 4	12 ± 2	11 ± 2
CRC_C	21 ± 5	10 ± 3	11 ± 2

[a] Black lamellae correspond to PBLG domains and white lamellae to PHF domains.

Transmission Electron Microscopy. Bright field imaging was performed on a CM100 Philips TEM operated at 80 kV (emission 2). All images were acquired on a SIS Morada CCD camera. Samples were embedded in a standard four components epoxy resin (46 wt % Epon 812, 28 wt % (dodecenylsuccinic anhydride) DDSA, 25% (nadic methyl anhydride) NMA, 1% 2,4,6-tris(dimethylaminomethyl)phenol) catalyst. In order to avoid diffusion of the resin components into the sample, the resin was precured 2 h at 70 °C before embedding the sample for 8 h at 70 °C. The samples were ultramicrotomed on a Reichert-Jung microtome at room temperature. 50 nm thick sections were collected on 300 hexagonal mesh copper grids (EMS G300H-Cu). Ruthenium tetraoxide (RuO_4) was used to stain the PBLG blocks in both the CRC and RRR series. A typical exposure time to the RuO_4 vapor was 15 min.

Small- and Wide-Angle X-ray Scattering. SAXS and WAXS spectra were acquired on a device consisting of a Bruker MICROSTAR microfocus rotating anode X-ray source with Montel Optics (Cu Kα radiation $\lambda = 1.54$ Å), where the beam was further collimated using four sets of four blade slits. The sample-to-detector distances of 1.5 and 0.45 m were used spanning a q range from 0.006 to 0.14 $Å^{-1}$ and from 0.02 to 0.8 $Å^{-1}$, respectively. Scattering intensities were measured using a 2-D area detector (Bruker AXS). The magnitude of the scattering vector is given by $q = (4\pi/\lambda) \sin \theta$, where 2θ is the scattering angle. Samples of about 100 μm were maintained between two Kapton sheets. Data treatment follows standard procedures for empty cell, detector response, and spatial distortion corrections.

Photoluminescence Experiments. The photoluminescence (PL) emission measurements were performed on a Perkin-Elmer LS50B luminescence spectrometer using a homemade sample holder. The fluorescence emission was detected in the direction normal to the excitation beam. The excitation wavelength was 350 nm, and the samples were casted on glass, following the annealing procedure described previously. The same samples were used to perform time-resolved PL decay measurements using the time-correlated single photon counting technique (TCSPC). The polymer films of few tens of micrometers were cast on glass substrates for observation. The fluorescence decay wavelength was set at 520 nm throughout the study. The number of the fluorescent photons was kept low relative to the number of start pulses (1% or less).

Results

Transmission Electron Microscopy. TEM images on the CRC sample series present a well-defined phase separation as shown in Figure 1a−c. Samples CRC_A and CRC_B exhibit a lamellar morphology, with a more polydisperse lamellae dimension in CRC_A sample than CRC_B. Sample CRC_C presents a rather disordered worm-type morphology in which lamellar ordering occurs locally with a very short persistence length of about 50 nm. To quantify the period and the lamellae dimensions, a systematic study previously described in literature[31] was performed. The data are presented in Table 2. Since RuO_4 was used as staining agent, the black domains are expected to be made of PBLG and the white ones of PHF. The periods measured for samples A, B, and C are respectively 35, 23, and 21 nm. On the other hand, TEM images from RRR series reveal black nanometer scale domains in a white matrix as shown in Figure 2a−c. Again, given that RuO_4 was used as staining agent,

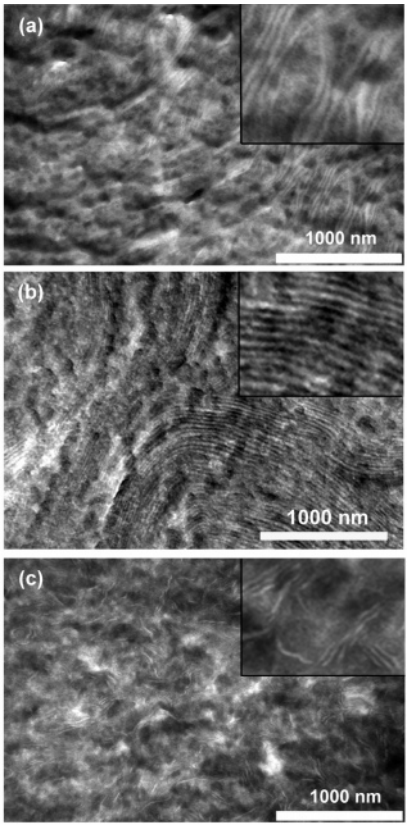

Figure 1. TEM micrographs obtained on RuO_4-stained samples CRC_A (a), CRC_B (b), and CRC_C (c). Insets give high-magnification zoom-up of the structure.

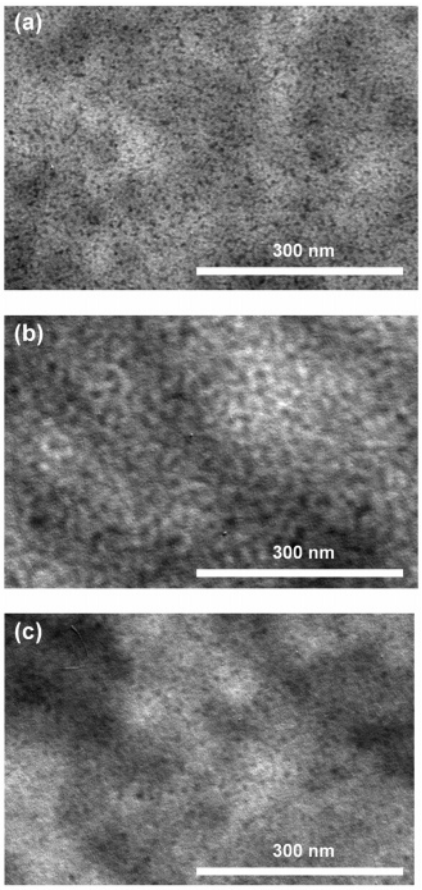

Figure 2. TEM micrographs obtained on RuO_4-stained samples RRR_A (a), RRR_B (b), and RRR_C (c).

the black domains are expected to be made of the PBLG and the white matrix of PHF. Characteristic sizes are extracted from the image by averaging 50 measurements of first neighbor black domains distance. The characteristic size measured for samples A, B, and C are respectively 9 $\pm$ 2, 17 $\pm$ 3.5, and 15 $\pm$ 3 nm. These results will then be discussed by means of WAXS and SAXS data.

Wide-Angle X-ray Scattering. In Figure 3a,b the large-angle X-ray diffraction spectra measured on samples in both conformations are shown. One major peak is present in all the spectra at about 0.47 $Å^{-1}$. This peak is the main feature on the scattering curves measured on the RRR series, whereas in the CRC series other important peaks arise at larger angles. The q-position of this peak corresponds to 1.33 nm in the direct space using the Bragg relation, $D = 2\pi/q$. This value is in good agreement with the α-helix−α-helix distance, 1.3 nm,[16,24,32,33] which is the predominant interaction in the rod−rod−rod conformation. 1.33 nm is also in good agreement with the lateral packing of the PHF block, i.e., 1.31 nm,[16] which is the major interchain interaction in coil−rod−coil form. We then attribute the peak to PBLG helix-to-helix interdistance in the RRR series (Figure 3a) and to PHF close packing in the CRC (Figure 3b). In both conformations, another peak is observed only on samples A and C spectra at a q-position of about 0.4 $Å^{-1}$. The TFA treatment does not suppress this peak. This scattering feature can be attributed to the lamellar spacing of β-sheets,[34] as it has been observed that short chains of PBLG, less than 20 units, present most likely both α-helices and β-sheets.[24] On the other hand, in Figure 3b, the q-positions of the large angle peaks in the CRC series are most likely the signature of an orthorhombic structure of the hairy PHF rods. Grell et al.[35] reported the crystallographic structure of polyfluorene with C8 alkyl chains. In that paper the authors propose that the molecules present an orthorhombic ribbon like structure with a 1.6 nm cross section (width) and a thickness of 0.44 nm, where the fluorene plane is normal to the ribbon width. The fact that in the present triblock copolymers the orthorhombic ordering of the PHF is observed only in the coil−rod−coil configuration is to be attributed to the release of packing restrictions characteristic for PBLG helices, the coil configuration allowing improved packing of PHF blocks.

Small-Angle X-ray Scattering. Scattering curves at low angles measured on the samples in both conformations are presented in Figure 4a,b using an Iq^2 vs q plot to facilitate the positioning of peaks. RRR series presents a large bump at 0.064, 0.067, and 0.035 $Å^{-1}$ respectively for samples A, B, and C. The $I(q) \sim q^{-4}$ general slope would suggest microphase separation from sharp interface (Porod's law); however, solely on the basis of the scattering data and considering the broad peaks, the possibility of a maximum arising upon concentration fluctuations cannot be fully ruled out. Therefore, we use evidence based on TEM images (Figure 2a−c) to further support microphase separation. The q-positions of the peaks correspond in the direct space to correlation distances of 9.5, 9.5, and 19 nm, which are correlated to PHF block contour lengths (see Table 1). On the other hand, all spectra measured on the CRC samples present a broad peak at small angles, positioned at 0.016, 0.027, and 0.023 $Å^{-1}$ for samples A, B, and C, respectively. These q-positions correspond in the direct space to correlation distances of 39, 23, and 27 nm, which are consistent with the TEM data presented in Table 2. The large bump visible at 0.063 $Å^{-1}$ on the CRC_A spectra is most likely a reminiscence of the RRR_A peak positioned at 0.064 $Å^{-1}$, due to a noncomplete unwinding of the α-helices.

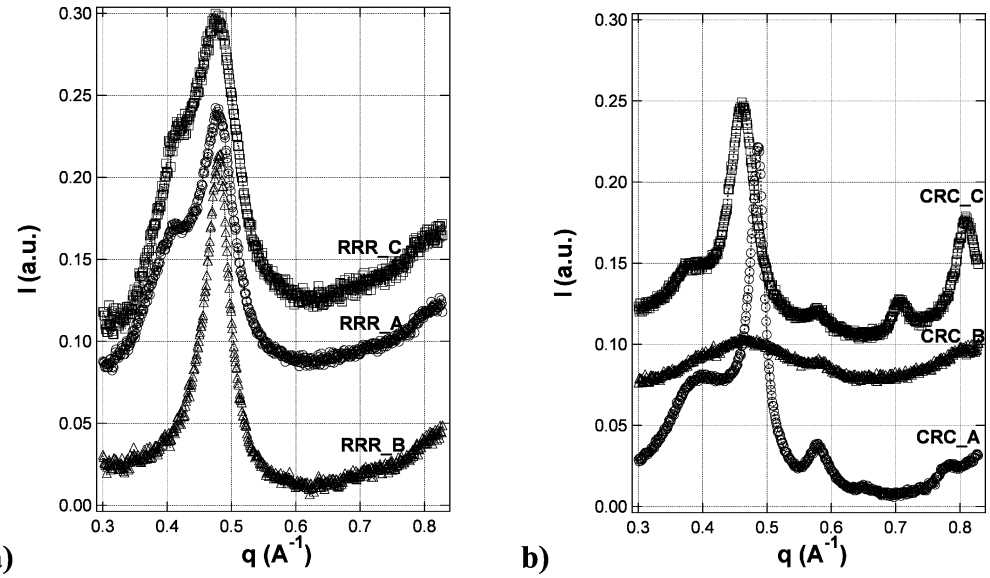

Figure 3. WAXS spectra acquired on samples casted from chloroform, RRR series (a), and casted from the TFA/chloroform mixture, CRC series (b). For both configurations circles, triangles, and squares represent respectively samples A, B, and C.

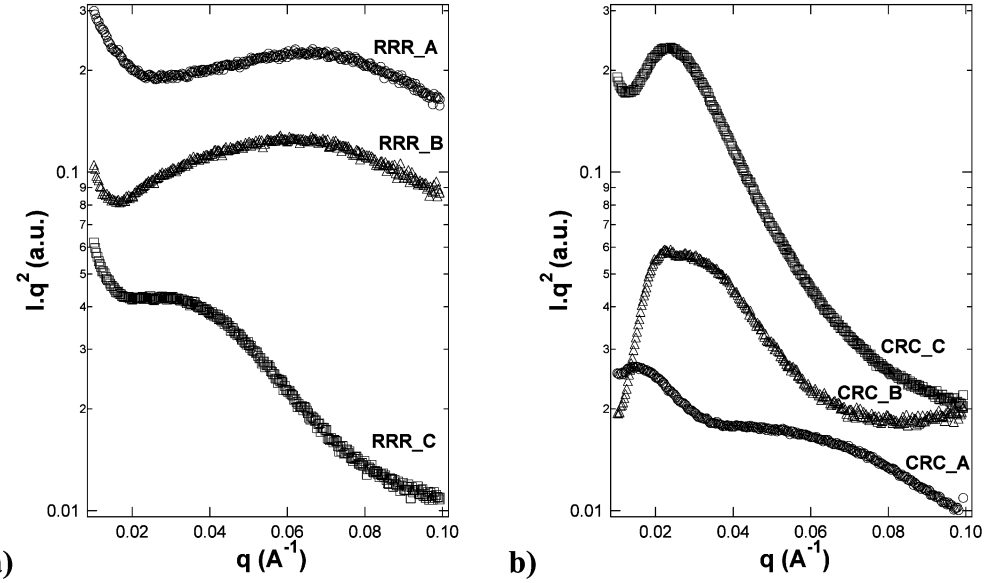

Figure 4. SAXS spectra acquired on samples casted from chloroform, RRR series (a), and casted from the TFA/chloroform mixture, CRC series (b). For both configurations circles, triangles and squares represent respectively samples A, B, and C.

Photoluminescence Spectra and Lifetime. Figure 5a shows the PL emission properties of sample B in both conformations, rod−rod−rod and coil−rod−coil. The PL emission spectra clearly show both a blue band with a peak around 435 nm and a broad, featureless, green band centered near 520 nm. A significant difference in the intensity of the blue band is observed among the B_RRR and B_CRC samples, which can be related to difference in their morphologies. The rod−rod−rod conformation presents a higher blue emission ratio relative to the green one. The blue emission of the two samples is relatively low compared to the green emission, which may be attributed to the annealing procedure.[27] Nevertheless, a significant difference in relative intensity of the blue emission is observed. Figure 5b presents the PL decay data fitted with a triple exponential ($n = 3$):

$$I(t) = y_0 + \sum_n a_n \exp\left(-\frac{t}{\tau_n}\right)$$

The fitting results are presented in Tables 3 and 4, corresponding respectively to the PBLG coil and rod conformation. In general, the PL decay of the coil conformation is significantly faster than the rod one. The main difference between the two is that the major component of the excited-state species decays faster in the coil conformation than the rod conformation, which is consistent with the observed difference in the steady-state PL data.

Discussion

Rod−Rod−Rod Conformation. At small length scale, below 2 nm, WAXS spectra show that the PBLG helices are aggregated in bundles. Such domains are observed by TEM with typical sizes of a few nanometers, which are in agreement with the contour length of the PBLG helices. At larger length scale, few tens of nanometers, SAXS spectra present large bumps, whose q-positions are correlated to the contour length of the middle PHF blocks. The proposed structural model, consistent with the experimental data, is presented in Scheme 2. A liquidlike

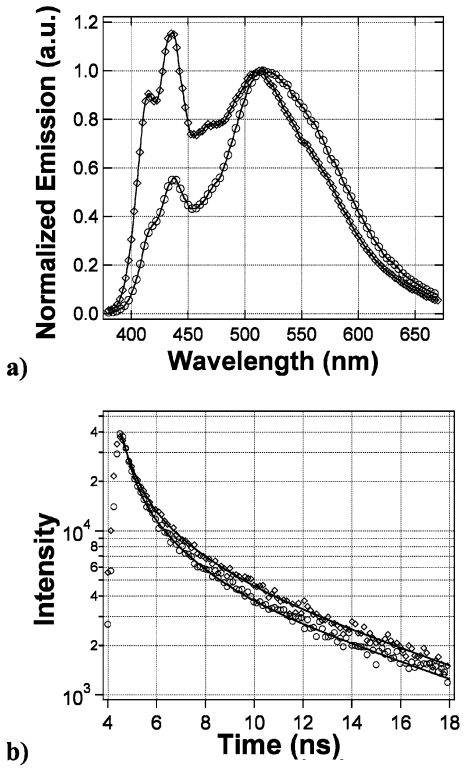

Figure 5. (a) Photoluminescence spectra measured on sample RRR_B (diamond) and CRC_B (circle) excited with a 350 nm wavelength light. The spectra are normalized to one at a wavelength of 514 nm. (b) Time-correlated single photon counting measurement on sample RRR_B (diamond) and CRC_B (circle). The solids lines correspond to the fits using a triple exponential.

Table 3. Fitting Parameters of the Time-Correlated Single Photon Counting Measured on the Coil−Rod−Coil Using a Triple-Exponential Decay ($\chi^2 = 1.07$ and $\sum a_n\tau_n = 2.09$ ns)

τ_n	a_n(%)	$a_n\tau_n$
$\tau_1 = 0.47$	$a_1 = 46$	0.21
$\tau_2 = 1.50$	$a_2 = 38$	0.57
$\tau_3 = 8.19$	$a_3 = 16$	1.31

Table 4. Fitting Parameters of the Time-Correlated Single Photon Counting Measured on the Rod−Rod−Rod Using a Triple-Exponential Decay ($\chi^2 = 1.11$ and $\sum a_n\tau_n = 2.47$ ns)

τ_n	a_n(%)	$A_n\tau_n$
$\tau_1 = 0.73$	$a_1 = 46$	0.33
$\tau_2 = 1.86$	$a_2 = 36$	0.67
$\tau_3 = 8.21$	$a_3 = 18$	1.47

ordering of small bundles of PBLG helices is considered. The black rods correspond to the PHF and the helices to the PBLG. In this sketch only the triblocks contained in-plane are shown, extra PBLG helices with connected PHF blocks need to be added pointing out of the drawing plan in order to maintain constant the overall density. It is important to note that the liquidlike ordering of the PBLG bundles and the distance between them are directly correlated with the triblock structure and mainly with the length of PHF middle block, in agreement with our SAXS/TEM study.

Coil−Rod−Coil Conformation. In this second series, TEM images and scattering spectra show clearly a phase separation between PBLG and PHF domains. Two things can count for this structural divergence between rod−rod−rod and coil−rod-coil systems: (i) first the superior flexibility of the coil−rod−coil copolymer and (ii) an increased conformational asymmetry between the rod and coil segments.[25] Furthermore, the correlation distances measured by SAXS are consistent with the TEM

Scheme 2. Schematic 2D Model of the PBLG−PHF−PBLG Triblock Copolymer Conformation in the Rod−Rod−Rod Form[a]

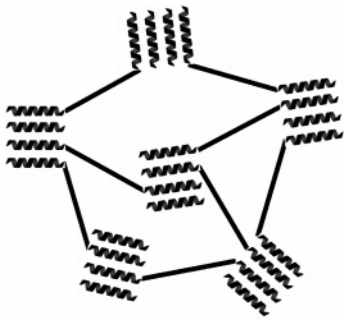

[a] The black rods correspond to the PHF and the gray helices to the PBLG. In this representation only the triblocks contained in one plane are fully presented.

observations. It is unambiguous from the TEM images that samples A and B present a lamellar morphology. The analysis of the sample C image is more uncertain, but lamellar domains are observed locally (see inset in Figure 1c). Therefore, a lamellar structure will be considered for all three samples to analyze the scattering data. Scheme 3a,b presents the lamellar model, with black rods corresponding to the PHF and the gray coils to the PBLG. In order to extract the unknown parameters (Table 5), the averaged volume occupied by both PBLG coils of each copolymer is calculated. This volume can be estimated by two ways: the first one is based on the chemical structure; knowing the molar mass, $M_{w,PBLG}$, and the density, ρ_{PBLG}, of the coils, one can write

$$V_{PBLG} = 2\frac{M_{w,PBLG}}{\rho_{PBLG}}N_a \quad (1)$$

with N_a the Avogadro number. The second way to get the PBLG volume is geometrical, knowing the PHF ribbon structure, as obtained by the WAXS experiment: the width, w, and the thickness, t, and considering a tilt angle of the PHF rods, θ (see Scheme 3b). These considerations lead to

$$V_{PBLG} = t'wl_{PBLG} \approx wt(D\sin^{-1}\theta - l_{PHF}) \quad (2)$$

with t' the apparent thickness of the PHF ribbon when a tilt angle of θ is present. l_{PBLG} is the lengths of the PBLG lamellae, whereas l_{PHF} corresponds to the PHF rods contour length. Note that there is not a factor 2 aside l_{PBLG}, since two PBLG coils have to fit in the same volume in order to respect the lamellar period, D, measured by SAXS.

Merging eqs 1 and 2 leads to

$$2\frac{M_{w,PBLG}}{\rho_{PBLG}}N_a \approx wt(D\sin^{-1}\theta - l_{PHF}) \quad (3)$$

θ is the only unknown value if we consider that the density of the PBLG coil in bulk remains close to 1.278, which is the density measured for PBLG in bulk when the helical secondary structure is present.[16] The width of the PHF ribbon, w, is given by the WAXS experiment and is found to be 1.33 nm. The value of its thickness, t, used for the calculation is 0.44 nm.[16,35] From θ, the lamellae thicknesses D_{PBLG} and D_{PHF} can be easily estimated using the following relations:

$$D_{PHF} = l_{PHF}\sin\theta$$
$$D_{PBLG} = l_{PBLG} = D - D_{PHF} \quad (4)$$

Table 5. Results from the SAXS and WAXS Spectra Analysis on the Coil−Rod−Coil Samples, Using the Lamellar Model

samples	w^a (nm)	t^b (nm)	$l_{PHF}{}^c$ (nm)	D^d (nm)	θ	D_{PBLG} (nm)	D_{PHF} (nm)	ϕ_{PBLG} (nm)
CRC_A	1.33	0.44	12.6	39	82.1	26.5	12.5	0.68
CRC_B	1.33	0.44	12.6	23	17.8	19.1	3.9	0.83
CRC_C	1.33	0.44	23.5	27	40	12	15	0.44

[a] w is the width of the ribbonlike shape of the PHF measured by WAXS. [b] t is the thickness of the ribbon, measured by WAXS.[16] [c] l_{PHF} is the contour length of the PHF rod blocks.[16] [d] D is the period measured by SAXS. θ, D_{PBLG}, and D_{PHF} are calculated from the CRC model. ϕ_{PBLG} is the PBLG volume fraction calculated from D_{PBLG} and D_{PHF}.

Scheme 3. (a) Schematic Model of the PBLG−PHF−PBLG Triblock Copolymer Conformation in the Coil−Rod−Coil Form; (b) Description of the Volume Occupied by a Single Triblock Copolymer[a]

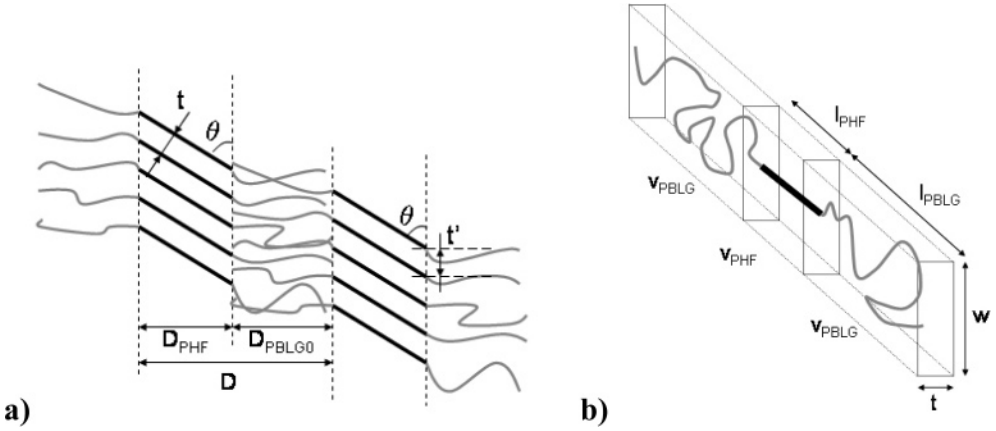

[a] The black rods correspond to the PHF rods and the gray coils to the PBLG.

Results of these calculations are presented in Table 5. The PBLG volume fraction values obtained through this basic model, 0.68, 0.83, and 0.44 for samples A, B, and C, respectively, are very close to those obtained more directly from the molar mass and the density, which are 0.66, 0.82, and 0.44, respectively. This confirms the validity of our topological lamellar model. The densities used for this calculation are 1.278 for the PBLG and 1.11 for the PHF. The latter value is evaluated using the crystallographic results from Grell et al.[35]

From the analysis of the data in Table 5, it appears as well that for an identical PHF block, samples A and B, the tilting angle of the rods increases with the coil molecular weight, as expected, in order to limit the stretching of the coil. On the other hand, a rather higher tilting angle is calculated for sample C compared to sample A which has a similar PBLG coil dimensions. The reduced WAXS scattering intensity measured on sample CRC_B can be attributed to the highly tilted conformation of PHF rods which may limit the ribbonlike structure formation.

In order to minimize the distance of the π-stacking interactions, only a limited number of positions will be allowed; these positions are the ones at which two aromatic rings are facing each other. Given the PHF monomer dimension, 0.835 nm,[35] considering a shift of 0, $^1/_2$, and 1 PHF monomer dimension, leads respectively to tilting angles of 90°, 44°, and 26°. These values are in good agreement with the tilt angles found for sample A, C, and B, respectively. A shift of half of a monomer unit was already proposed by Grell et al. in ref 35 to explain their crystallographic data. Furthermore, Sary et al. observed shifts of integer values on poly(phenylenevinylene) (PPV) units in PPV−PS rod−coil block copolymers, also due to maximization of π-stacking interactions.[31] In conclusion, the lamellar periods measured by TEM are in good agreement with the ones from SAXS. However, we cannot conclusively compare the dimensions of the PBLG and PHF lamellae obtained by TEM analysis and the present model due to the weak contrast on the TEM images, which makes challenging the achievement of a perfect focusing of the images.

The blue band in the PL emission spectra of the samples is due to intrinsic emission of the PHF block, and this is in accord with prior observations on spin-coated thin films.[16] We note that the dominant peak of the blue band in both spectra of our annealed samples (e.g., Figure 5a) corresponds to the 0−1 transition in the emission spectrum. In contrast, the prior thin film samples without the prolonged annealing of the current study had the 0−0 emission transition as the dominant peak in the PL emission spectrum.[16] Thus, the increased order of the annealed samples results in some changes in the blue band of the PL spectrum. This difference in the blue region of the PL emission spectra of the RRR and CRC samples is consistent with the molecular packing structures proposed, since the isolated PHF blocks (Scheme 2) should have a more intense blue band than those packed together (Scheme 3). Thus, a correlation between the observed morphology and photoluminescence is implicated.

The observed green band in the PL emission spectra of the PBLG−PHF−PBLG triblock copolymers could originate from two possible sources. First, the extended annealing of the samples would suggest the presence of fluorenone defects.[36] In that case, the green band should not vary with morphology of the block copolymer samples. Alternatively, the self-assembly of the PHF blocks in the coil−rod−coil conformation (Scheme 3) could enhance the formation of excimers. However, we believe that fluorenone defects best explain the observed PL emission properties of the annealed block copolymers.

Conclusions

The bulk ordering of a series of three hybrid triblock copolymers (BLG*m*-HF*n*-BLG*m*) containing poly(9,9-dihexylfluorene-2,7-diyl) (PHF) and poly(γ-benzyl-L-glutamate) (PBLG) has been investigated using a combination of TEM imaging (real space) and X-ray scattering (reciprocal space). The copolymers exhibit two different conformations: rod−rod−rod and coil−rod−coil as a consequence of a controllable rod-to-coil transition of the polypeptidic helices. Experimental data show that the coil−rod−coil form of the copolymer leads to lamellar ordering,

whereas the rod−rod−rod systems remain in a clusterlike structure. Two things can account for the structural divergence between rod−rod−rod and coil−rod−coil systems: (i) first the larger flexibility of the coil−rod−coil copolymer and (ii) increased conformational asymmetry between the rod and coil segments. The dimensions of the individual lamellar layers have been extracted using a simple lamellar model, leading to the value of the tilting angle of the PHF rods. This rod tilting, which varies systematically in the three block copolymers studied, permits to release the PBLG coil stretching and was quantified in shifts along the PHF contour length corresponding to 0, $^1/_2$, and 1 PHF repeating units. The observed photoluminescence spectra and decay were found to vary substantially between rod−rod−rod and coil−rod−coil configurations, and their systematic changes could be correlated to the morphology of triblock copolymers.

Acknowledgment. The authors thank Gebert Ruf Stiftung for financial support. Panu Hiekkataipale is thanked for his help in performing the SAXS and WAXS experiments. Prof. H. Girault (EPFL) is kindly acknowledged for support with PL measurements. Work at the University of Washington was supported by the U.S. Army Research Office DURINT Program and the NSF STC-CMDITR (DMR-0120967).

References and Notes

(1) Semenov, A. N. *Mol. Cryst. Liq. Cryst.* **1991**, *209*, 191−199.
(2) Reenders, M.; ten Brinke, G. *Macromolecules* **2002**, *35*, 3266−3280.
(3) Matsen, M. W.; Barrett, C. *J. Chem. Phys.* **1998**, *109*, 4108−4118.
(4) Bates, F. S.; Fredrickson, G. H. *Annu. Rev. Phys. Chem.* **1990**, *41*, 525−557.
(5) Bates, F. S.; Fredrickson, G. H. *Phys. Today* **1999**, *52*, 32−38.
(6) Leibler, L. *Macromolecules* **1980**, *13*, 1602−1617.
(7) Sary, N.; Rubatat, N.; Brochon, C.; Hadziioannou, G.; Ruokolainen, J.; Mezzenga, R. *Macromolecules* **2007**, *40*, 6990−6997.
(8) Duchs, D.; Sullivan, D. E. *J. Phys.: Condens. Matter* **2002**, *14*, 12189−12202.
(9) Pryamitsyn, V.; Ganesan, V. *J. Chem. Phys.* **2004**, *120*, 5824−5838.
(10) Lee, H. F.; Sheu, H. S.; Jeng, U. S.; Huang, C. F.; Chang, F. C. *Macromolecules* **2005**, *38*, 6551−6558.
(11) Borsali, R.; Lecommandoux, S.; Pecora, R.; Benoit, H. *Macromolecules* **2001**, *34*, 4229−4234.
(12) Li, K.; Wang, Q. *Chem. Commun.* **2005**, 4786−4788.
(13) Xiao, X.; Fu, Y. Q.; Zhou, J. J.; Bo, Z. S.; Li, L.; Chan, C. M. *Macromol. Rapid Commun.* **2007**, *28*, 1003−1009.
(14) Raphael, E.; Degennes, P. G. *Makromol. Chem., Macromol. Symp.* **1992**, *62*, 1−17.
(15) Pron, A.; Rannou, P. *Prog. Polym. Sci.* **2002**, *27*, 135−190.
(16) Kong, X. X.; Jenekhe, S. A. *Macromolecules* **2004**, *37*, 8180−8183.
(17) Schmidt, C. E.; Shastri, V. R.; Vacanti, J. P.; Langer, R. *Proc. Natl. Acad. Sci. U.S.A.* **1997**, *94*, 8948−8953.
(18) (18) Wallace, G. G.; Kane-Maguire, L. A. P. *Adv. Mater.* **2002**, *14*, 953−960.
(19) Fan, C. H.; Wang, S.; Hong, J. W.; Bazan, G. C.; Plaxco, K. W.; Heeger, A. J. *Proc. Natl. Acad. Sci. U.S.A.* **2003**, *100*, 6297−6301.
(20) de Groot, K.; Feyen, J.; de Visser, A. C.; van de Ridder, G.; Bantjes, A. *Kolloid Z. Z. Polym.* **1971**, *246*, 578−579.
(21) Roots, J.; Edsman, K.; Nyström, B. *Makromol. Chem.* **1980**, *181*, 2395−2400.
(22) Duke, R. W.; Dupre, D. B.; Hines, W. A.; Samulski, E. T. *J. Am. Chem. Soc.* **1976**, *98*, 3094−3101.
(23) Crespo, J. S.; Lecommandoux, S.; Borsali, R.; Klok, H. A.; Soldi, V. *Macromolecules* **2003**, *36*, 1253−1256.
(24) Klok, H. A.; Langenwalter, J. F.; Lecommandoux, S. *Macromolecules* **2000**, *33*, 7819−7826.
(25) Lecommandoux, S.; Achard, M. F.; Langenwalter, J. F.; Klok, H. A. *Macromolecules* **2001**, *34*, 9100−9111.
(26) Neher, D. *Macromol. Rapid Commun.* **2001**, *22*, 1366−1385.
(27) Kulkarni, A. P.; Jenekhe, S. A. *Macromolecules* **2003**, *36*, 5285−5296.
(28) Chen, P.; Yang, G. Z.; Liu, T. X.; Li, T. C.; Wang, M.; Huang, W. *Polym. Int.* **2006**, *55*, 473−490.
(29) Tung, Y. C.; Wu, W. C.; Chen, W. C. *Macromol. Rapid Commun.* **2006**, *27*, 1838−1844.
(30) Lu, S.; Liu, T. X.; Ke, L.; Ma, D. G.; Chua, S. J.; Huang, W. *Macromolecules* **2005**, *38*, 8494−8502.
(31) Sary, N.; Mezzenga, R.; Brochon, C.; Hadziioannou, G.; Ruokolainen, J. *Macromolecules* **2007**, *40*, 3277−3286.
(32) Elliot, A. In *Poly(α-amino acids): Protein Models for Conformational Studies*; Marcel Dekker: New York, 1967.
(33) Minich, E. A.; Nowak, A. P.; Deming, T. J.; Pochan, D. J. *Polymer* **2004**, *45*, 1951−1957.
(34) Floudas, G.; Papadopoulos, P.; Klok, H.-A.; Vandermeulen, G. W. M.; Rodriguez-Hernandez, J. *Macromolecules* **2003**, *36*, 3673−3683.
(35) Grell, M.; Bradley, D. D. C.; Ungar, G.; Hill, J.; Whitehead, K. S. *Macromolecules* **1999**, *32*, 5810−5817.
(36) Kulkarni, A. P.; Kong, X. X.; Jenekhe, S. A. *J. Phys. Chem. B* **2004**, *108*, 8689−8701.
(37) Block, H. *Poly(γ-benzyl-L-glutamate) and Other Glutamic Acid Containing Polymers*; Gordon and Breach: New York, 1983.

MA702278A